SUPPORTING INFORMATION

Interaction of intramembrane metalloprotease SpoIVFB with substrate Pro-σ^K

Sabyasachi Halder, Daniel Parrell, Douglas Whitten, Michael Feig, and Lee Kroos[1]

Department of Biochemistry and Molecular Biology, Michigan State University, East Lansing, MI 48824

[1]To whom correspondence should be addressed. E-mail: kroos@msu.edu.

METHODS

Purification of SpoIVFB and SpoIVFB A12. Cells were harvested and resuspended in 40 mL lysis buffer. The His-tagged proteins were purified as described (1) with the following modifications. The membrane pellet was resuspended in 40 mL detergent buffer, rotated 1 h at 4°C to allow membrane solubilization, and centrifuged at 150,000 × *g* for 75 min at 12°C. The supernatant was added to 1 mL Talon superflow metal affinity resin that had been equilibrated with PBS containing 1% sarkosyl and 0.5% DM. The mixture was rotated at room temperature for 1 h. The cobalt resin was sedimented by centrifugation at 708 × *g* for 2 min at 4°C, then the resin was washed with 5 mL each of PBS containing 150 mM NaCl and 10% glycerol plus first 0.3% sarkosyl and 0.3% DM, second 0.3% DM, and third 0.3 % DM and 20 mM imidazole. The resin was eluted with 3 mL PBS containing 150 mM NaCl, 10 % glycerol, 0.3% DM, and 400 mM imidazole. The eluted material was concentrated to 0.5 mL using an Amicon Ultra centrifugal filter device with a 10-kDa cut-off (Millipore). The sample was loaded onto a 1.0 cm × 30 cm Superdex 200 gel filtration column (GE Healthcare) that had been equilibrated with PBS containing 150 mM NaCl, 5% glycerol, and 0.3% DM. The column was eluted with the same buffer at 0.5 mL/min and 0.5-mL fractions were collected. Samples were subjected to SDS/PAGE, the gel was stained with Coomassie blue, and 3-4 fractions containing the most SpoIVFB were combined, concentrated to 0.5 mL as described above, and stored at -80°C.

Purification of the SpoIVFB·Pro-σ^K Complex. Cells (7.5 g) were resuspended in 40 mL lysis buffer. The His-tagged complex was purified as described (2) with the following modifications. The membrane pellet was resuspended in 40 mL PBS containing 1 mM Pefabloc SC, 5 mM 2-mercaptoethanol, 10% glycerol, and 1% *n*-dodecyl-β-D-maltoside (DDM) (Anatrace), rotated 1

h at 4°C to allow membrane solubilization, and centrifuged at 150,000 × *g* for 75 min at 12°C. The supernatant was added to 1 mL Talon superflow metal affinity resin that had been equilibrated with PBS containing 0.1% DDM, 5 mM 2-mercaptoethanol, and 10% glycerol. The mixture was rotated for 1 h at room temperature. The cobalt resin was sedimented by centrifugation at 708 × *g* for 2 min at 4°C, then the resin was washed twice with 5 mL equilibration buffer and once with 5 mL PBS containing 150 mM NaCl, 10% glycerol, 0.1% DDM, and 40 mM imidazole. The resin was eluted with 3 mL of PBS containing 150 mM NaCl, 10% glycerol, 0.1% DDM, and 400 mM imidazole. The eluted material was concentrated to 0.5 mL and loaded onto a gel filtration column as described above except 0.02% DDM was substituted for 0.3% DM in the column buffer. The column was eluted at 0.5 mL/min and 0.5-mL fractions were collected. Samples were subjected to SDS/PAGE, the gel was stained with Coomassie blue, and 3-4 fractions containing the most SpoIVFB and Pro-σ^K were combined, concentrated to 0.5 mL as described above, and stored at -80°C.

In-gel Protease Digestion and Peptide Purification. Cross-linked products were digested in-gel as described (3) with the following modifications. Gel bands were dehydrated using 100% acetonitrile and incubated with 10 mM DTT in 100 mM ammonium bicarbonate, pH~8, at 56°C for 45 min, dehydrated again and incubated in the dark with 50 mM iodoacetamide in 100 mM ammonium bicarbonate for 20 min. Gel bands were then washed with ammonium bicarbonate and dehydrated again. Sequencing-grade modified typsin or chymotrypsin was prepared at 0.01 ug/uL in 50 mM ammonium bicarbonate and ~50 uL of this was added to each gel band so that the gel was completely submerged. Bands were then incubated at 37°C overnight. Peptides were extracted from the gel by water bath sonication in a solution of 60% ACN/1% TCA and

vacuum dried to ~2 uL. Peptides were then resuspended in 2% acetonitrile/0.1% TFA to 25 uL. From this, 5 uL was automatically injected by a Thermo EASYnLC 1000 onto a Thermo Acclaim PepMap RSLC 0.075 mm x 150 mm C18 column and eluted over 60 min with a gradient of 2% buffer B to 30% buffer B in 49 min, ramping to 100% buffer B at 50 min and held at 100% buffer B for the duration of the run (buffer A = 99.9% water/0.1% formic acid and buffer B = 99.9% acetonitrile/0.1% formic acid).

Mass Spectrometry and Data Analysis. Eluted peptides were sprayed into the mass spectrometer using a FlexSpray ion source. Survey scans were obtained in the Orbi trap (70,000 resolution, determined at m/z 200) and the top ten ions in each survey scan were then subjected to automatic higher-energy collisional dissociation (HCD) with fragment spectra acquired at 17,500 resolution. The resulting MS/MS spectra were converted to peak lists using Mascot Distiller v2.5.1.0 (www.matrixscience.com) and searched using the Mascot searching algorithm v2.4, against a protein database containing the target protein sequences with *E. coli* protein sequences (both downloaded from NCBI, www.ncbi.nlm.nih.gov) for background and appended with common laboratory contaminants. The Mascot output was then analyzed using Scaffold v4.3.4 (www.proteomesoftware.com) to probabilistically validate protein identifications. Assignments validated using the Scaffold 1% false discovery rate confidence filter were considered true. For cross-link assignments, remaining unmatched spectra from the initial Mascot analyses were exported from Scaffold as processed peak lists and searched against the target protein sequences and common laboratory contaminants using StavroX (4).

Modeling of the SpoIVFB·Pro-σ^K complex. The N-terminal membrane domain of SpoIVFB (residues 1-209) was modeled by homology using the mjS2P structure (PDB code: 3B4R) as a template (22% sequence identity and E-value of $5.6*10^{-29}$) (5). MODELLER (6) was used in conjunction with the MMTSB Tool Set (7). The crystal structure contains two chains that differ in their conformations (5). The A chain is more open towards the active site and has a more ordered C-terminal helix. The B chain is more closed and exhibits more disorder towards the end of the C-terminal helix. Models for SpoIVFB were built based on both chains. The tetramer that was ultimately built consisted of two subunits based on the A structure (called chains A and C in the model), presumed to be able to bind to Pro-σ^K, and two subunits based on the B structure (called chains B and D), presumed to be substrate-free, in order to be consistent with experimental evidence that a catalytically-inactive SpoIVFB tetramer complexes with only two bound Pro-σ^K substrates (called chains X and Y in the model) (2).

The mjS2P crystallographic dimer places the C-termini of each subunit opposite of each other (5). However, this antiparallel arrangement is not compatible with experimental data for the membrane topology of SpoIVFB (8) and would not allow tetramerization of the C-terminal CBS domains since only two subunits each would be on either side of the membrane. Therefore, one of the SpoIVFB N-terminal domains was rotated to a parallel orientation followed by rotation around the *z*-axis to build a dimer with approximate shape complementarity. A tetramer was subsequently built by rotating the initial dimer around the *z*-axis, the membrane normal, by 180^o followed by translation along the *x*- and *y*-axes until overlap of the two dimers was avoided. Care was taken to have all four active sites face outwards since otherwise Pro-σ^K binding and product release would be impossible or seriously hindered. The goal of this initial step was to place the SpoIVFB N-terminal domains at reasonable initial positions but with extra distance to

obtain an initial conformation that could be refined further. The initial model was reduced to Cα positions and subjected to molecular dynamics simulations. The Cα-based model consisted of harmonic bonds between subsequent residues to maintain a distance of 3.8 Å in addition to a Lennard-Jones potential (radius 3.5 Å) to avoid overlap of Cα particles. Harmonic restraints were applied to keep each of the subunits rigid, minimize the distance between the centers of mass of each subunit, and maintain each subunit to be aligned with the membrane normal and centered around z=0. The restrained simulations were repeated many times with different initial velocity distributions. The resulting structures were clustered based on overall RMSD. Eight clusters were identified with populations of 268, 250, 131, 112, 76, 70, 62, and 21 elements. The representative structure from the most populated cluster was selected as a likely tetrameric model. We note that the representative structure of the second-largest cluster was only 3 Å from the selected model while the largest deviation was found for the representative structure of the smallest cluster with about 5 Å. Therefore, the subsequent modeling is not expected to be especially sensitive to the selected cluster.

The C-terminal domain of SpoIVFB (residues 214-279) is homologous to a single CBS domain (9). Available structures feature CBS domains either as dimers or as disc-like tetramers. There are two major tetramer configurations, only one of which is fully compatible with an N-terminal tetramer consisting of four membrane-bound subunits on one side of the disc-like structure. An example of this configuration is given by the CBS-domain protein TM0935 from *Thermotoga maritima* (PDB code: 1O50) (10), which was used as the structure template for building a tetramer for the C-terminal part of SpoIVFB (13% sequence identity and E-value of $5.6*10^{-5}$).

The SpoIVFB model was completed by first positioning the C-terminal tetrameric CBS disc beneath the N-terminal membrane-localized tetramer. Flexible linkers for residues 210-213 were then added to connect both sections of SpoIVFB.

To model Pro-σ^K, the structure of the RNA-polymerase sigma subunit domain 2 from *Thermus aquaticus* (PDB code: 3UGO) (11) was used as the template to build a structure for residues 34-106 of Pro-σ^K (40% sequence identity and E-value of $1.2*10^{-10}$). The missing N-terminal residues 1-33 were added as an extended chain since structural information is not available for the Pro sequence. The exact positioning of Pro-σ^K with respect to SpoIVFB is unclear and in an initial model two copies of Pro-σ^K were placed near the A and C chains of SpoIVFB outside the membrane plane and with the N-terminus oriented towards the protease active site.

The modeling described above only resulted in a very approximate initial model since the tetramerization interface of the SpoIVFB membrane domains, the interaction of the SpoIVFB membrane domains and CBS domains, and the interaction of SpoIVFB with Pro-σ^K were unclear. Constraints from cross-linking experiments were used to further refine the initial model via molecular dynamics simulations of a coarse-grained representation (only Cα positions) in the presence of various restraint potentials that are detailed in the following:

1. The membrane domains (residues 1-200) of the two Pro-σ^K-binding SpoIVFB chains A and C were harmonically restrained to their initial position (using a force constant of 2.0 kcal/mol/Å^2). This restraint anchors the membrane domains in space.
2. The membrane domains of SpoIVFB chains B and D were restrained with respect to their overall structure (using a force constant of 4.0 kcal/mol/ Å^2) but not fixed in space, to allow for some flexibility in adjusting the initial tetramer model to the presence of the

CBS domains and Pro-σ^K. Additional restraints between the active sites of different chains and between residues at the 'top' of the tetramer (opposite the CBS domain) kept chains B and D close to the initial tetramer model since there are no other forces in the modeling protocol that would keep SpoIVFB subunits together or in the membrane otherwise.

3. The tetrameric CBS domains of SpoIVFB (residues 220-272) were restrained together to maintain their internal tetrameric structure (using a force constant of 2.0 kcal/mol/Å^2) while allowing only rigid body motions of the entire tetramer.
4. The interdomain linkers of SpoIVFB (residues 201-219) were fully flexible.
5. The two Pro-σ^K chains X and Y were restrained to maintain their internal structure for parts of the template-based model (residues 38-122 and residues 29-37 using a force constant of 5.0 kcal/mol/Å^2) allowing for free sampling of the helix from 29-37 relative to the rest of the model and a fully flexible N-terminus.
6. Cross-linking data was incorporated in the form of flat-bottom potentials typically used for NOE restraints. Table S3 gives the restraints that were implemented and their distance ranges.
7. Residues H43, H47, and D137 of SpoIVFB were restrained to bind a zinc ion at the active site and residue E44 was restrained to be able to activate a water molecule to cleave the peptide bond between residues S21 and Y22 of Pro-σ^K (12-14).
8. SpoIVFB chains A and C interact with Pro-σ^K chains X and Y, respectively. No restraints were applied between SpoIVFB chains B and D, and Pro-σ^K. Also, no restraints were applied between SpoIVFB chains except the weak restraints mentioned above to maintain the overall tetramer. The restraints on the SpoIVFB interdomain linker

(residues 200-220) from cross-linking data were not applied uniformly to all chains because the CBS domain tetramer orientation requires a more extended linker for the B and D chains in order to satisfy the restraints for the A and C chains (Table S2).

Using these restraints models were initially minimized for 1,000 steps using an adopted-basis Newton-Raphson scheme. Subsequently, 50,000 steps of molecular dynamics were carried out at 1,000 K in an NVT ensemble followed by another round of minimization over 100,000 steps. The temperature was maintained by periodically reassigning velocities and an integration time step of 2 fs was used. In the Cα-based model, bonds between adjacent beads were harmonically restrained to 3.8 Å using a force constant of 100 kcal/mol/$Å^2$. Hydrophobic (Ile, Leu, Phe, Trp, Gly, Pro, Val, Met, Cys, Ala) and polar (Lys, Arg, Asp, Glu, Ser, Thr, His, Tyr, Gln, Asn) beads were distinguished by different Lennard-Jones parameters with ε=0.05 for polar residues and ε=0.2 for hydrophobic residues. R_{min} was set to 3.7 Å for both types of beads. A charge of -0.1 was applied to acidic residues and a charge of 0.1 to basic residues. All beads had a mass of 50 amu. Non-bonded interactions were switched to zero between 16 and 18 Å and a non-bonded list cutoff of 20 Å was applied. While zinc was not present in the initial modeling, it was included in the restraint-based optimization of the complete Cα-based model to facilitate later conversion to an atomistic model. To hold the zinc atom in place, it was tethered to residues 43, 47, and 137 in each of the four subunits at distances of 6.4, 6.4, and 4.8 A using harmonic restraints with a force constant of 1.0 kcal/mol based on the position of the Zn ion in the mjS2P template structure relative to the Cα atoms. The minimization-MD-minimization protocol was repeated 100 times but because of the restraints the structure varied little (within 2-4 Å RMSD over the entire complex) with most of the variation involving the (unrestrained) N-terminus of Pro-σ^K and the linker between the membrane and CBS domains of SpoIVFB (see Fig. S12). The

variation in the models was well within the expected overall accuracy of the model (about 5 Å) and a representative structure was selected as the final model for further analysis.

The final model was then reconstructed to atomistic detail using the MMTSB Tool Set (7).

REFERENCES

1. Zhou R, Cusumano C, Sui D, Garavito RM, & Kroos L (2009) Intramembrane proteolytic cleavage of a membrane-tethered transcription factor by a metalloprotease depends on ATP. *Proc. Natl. Acad. Sci. USA* 106:16174-16179.
2. Zhang Y, *et al.* (2016) Complex formed between intramembrane metalloprotease SpoIVFB and its substrate, Pro-σ^K. *J. Biol. Chem.* 291:10347-10362.
3. Shevchenko A, Wilm M, Vorm O, & Mann M (1996) Mass spectrometric sequencing of proteins silver-stained polyacrylamide gels. *Anal. Chem.* 68(5):850-858.
4. Götze M, *et al.* (2012) StavroX - a software for analyzing crosslinked products in protein interaction studies. *J. Am. Soc. Mass Spectrom.* 23:76-87.
5. Feng L, *et al.* (2007) Structure of a site-2 protease family intramembrane metalloprotease. *Science* 318(5856):1608-1612.
6. Sali A & Blundell TL (1993) Comparative protein modelling by satisfaction of spatial restraints. *J. Mol. Biol.* 234(3):779-815.
7. Feig M, Karanicolas J, & Brooks CL, 3rd (2004) MMTSB Tool Set: enhanced sampling and multiscale modeling methods for applications in structural biology. *J. Mol. Graph Model* 22(5):377-395.
8. Green D & Cutting S (2000) Membrane topology of the *Bacillus subtilis* Pro-σ^K processing complex. *J. Bacteriol.* 182:278-285.

9. Kinch LN, Ginalski K, & Grishin NV (2006) Site-2 protease regulated intramembrane proteolysis: sequence homologs suggest an ancient signaling cascade. *Protein Sci.* 15(1):84-93.
10. Miller MD, *et al.* (2004) Crystal structure of a tandem cystathionine-β-synthase (CBS) domain protein (TM0935) from *Thermotoga maritima* at 1.87 Angstrom resolution. *Proteins* 57(1):213-217.
11. Feklistov A & Darst SA (2011) Structural basis for promoter-10 element recognition by the bacterial RNA polymerase sigma subunit. *Cell* 147(6):1257-1269.
12. Kroos L, Kunkel B, & Losick R (1989) Switch protein alters specificity of RNA polymerase containing a compartment-specific sigma factor. *Science* 243:526-529.
13. Rudner D, Fawcett P, & Losick R (1999) A family of membrane-embedded metalloproteases involved in regulated proteolysis of membrane-associated transcription factors. *Proc. Natl. Acad. Sci. USA* 96:14765-14770.
14. Yu Y-TN & Kroos L (2000) Evidence that SpoIVFB is a novel type of membrane metalloprotease governing intercompartmental communication during *Bacillus subtilis* sporulation. *J. Bacteriol.* 182:3305-3309.
15. Zhou R & Kroos L (2004) BofA protein inhibits intramembrane proteolysis of pro-σ^K in an intercompartmental signaling pathway during *Bacillus subtilis* sporulation. *Proc. Natl. Acad. Sci. USA* 101(17):6385-6390.
16. Kunkel B, Sandman K, Panzer S, Youngman P, & Losick R (1988) The promoter for a sporulation gene in the *spoIVC* locus of *Bacillus subtilis* and its use in studies of temporal and spatial control of gene expression. *J. Bacteriol.* 170:3513-3522.

17. Kunkel B, Kroos L, Poth H, Youngman P, & Losick R (1989) Temporal and spatial control of the mother-cell regulatory gene *spoIIID* of *Bacillus subtilis*. *Genes Dev.* 3:1735-1744.

Table S1 Chemically Cross-linked Peptides of the SpoIVFB·Pro-σ^K Complex

Cross-links between SpoIVFB and Pro-σ^K									
Cross-linker[a]	SpoIVFB Peptide[b]	Pro-σ^K Peptide	SpoIVFB Residue	Pro-σ^K Residue	Score[c]	Deviation (ppm)[d]	Charge[e]	Mass[f]	Times Observed
DSS	I**K**R	**K**FENTGEDAEDLISIGTIGLIK	K59	K69	322	-0.51	3	2917	3
BS3	I**K**R	**K**FENTGEDAEDLISIGTIGLIK	K59	K69	295	-0.8	3	2917	2
AMAS	**C**R	LVAHIV**KK**	C201[g]	K68 or K69	66	0.16	3	1322	2
DSS	YYG**K**NR	YLELMA**K**GDEHAR	K217	K46	252	-4.88	3	2470	1
DSS	YYG**K**NR	**K**YLELMAK	K217	K39	116	-3.03	2	1933	1
DSS	YYG**K**NR	**K**YLELMAKGDEHAR	K217	K39	83	-3.34	3	2598	1
Sulfo-SMCC	G**C**K	NNAFPQPLSSSEE**KK**YLELMAK	C246	K38 or K39	71	-1.44	4	3050	1
Sulfo-SMCC	G**C**K	**K**FENTGEDAEDLISIGTIGLIK	C246	K69	395	-2.46	3	2888	3
Sulfo-SMCC	G**C**K	GIESYSAG**K**GTK	C246	K99	86	-1.31	3	1723	1
Sulfo-SMCC	G**C**K	GT**K**LATYAAR	C246	K102	75	-1.59	2	1577	1
$BM(PEG)_2$	G**C**K	**C**IENEILMHLR	C246	C110	85	-0.81	3	2001	4
Cross-links within SpoIVFB									
Cross-linker	Peptide 1	Peptide 2	Residue 1	Residue 2	Score	Deviation (ppm)	Charge	Mass	Times Observed
DTSSP	MNKWLDLIL**K**	NRELE**K**	K10[h]	K223	81	-4.47	3	2235	2
Sulfo-SMCC	QLPFQ**K**AHR	G**C**K	K154	C246	81	-1.02	4	1650	2
AMAS	QLPFQ**K**AHR	**C**RHYIHVR	K154	C201[g]	21	-3.29	3	2344	1
DSS	YYG**K**	NRELE**K**	K217	K223	173	-3.88	3	1456	1
DSS	YYG**K**NR	ELE**K**	K217	K223	72	-3.88	3	1456	1
Sulfo-SMCC	YYG**K**NR	G**C**K	K217	C246	86	-1.05	2	1326	3
BS3	YYG**K**	LLPLTVKAEDKVYHVMAEFKRGB**K**	K217	K247	66	1.23	3	3516	1
DSS	ELE**K**LLPLTVK	AEDKVYHVMAEF**K**R	K223	K243	86	-0.83	4	3143	2
DSS	ELE**K**LLPLTVK	VYHVMAEF**K**R	K223	K243	75	-4.7	4	2716	1
Sulfo-SMCC	ELE**K**LLPLTVK	G**C**K	K223	C246	733	-1.7	2	1808	10
Sulfo-SMCC	NRELE**K**LLPLTVK	G**C**K	K223	C246	97	-1.35	4	2078	1
DSS	ELE**K**LLPLTVK	SGQ**K**LSQLDENEVLHAYFADKR	K223	K258	331	-4.33	4	3968	3
BS3	LLPLTV**K**	AED**K**	K230	K234	66	-0.25	2	1383	1
Sulfo-SMCC	LLPLTV**K**AEDK	G**C**K	K230	C246	139	-1.98	3	1752	3

Sulfo-SMCC	AED**K**VYHVMAEFK	G**C**K	K234	C246	129	-1.56	4	2248	3
Sulfo-SMCC	AED**K**VYHVMAEFKR	G**C**K	K234	C246	64	0.98	4	2264	1
Sulfo-SMCC	G**C**K	HPIIIE**K**SGQ**K**	C246	K254 or K258	277	-2.77	2	1775	9
Sulfo-SMCC	G**C**K	SGQ**K**LSQLDENEVLHAYFADKR	C246	K258	220	-2.46	4	3074	2
Sulfo-SMCC	G**C**KHPIIIEK	SGQ**K**	C246	K258	62	-3.21	2	1775	2
Sulfo-SMCC	RG**C**K	LSQLDENEVLHAYFAD**K**	C246	K275	91	-4.26	3	2673	2
Sulfo-SMCC	G**C**K	LSQLDENEVLHAYFAD**K**R	C246	K275	85	-4.26	3	2673	2
BS3	HPIIIE**K**	SGQ**K**	K254	K258	66	-0.41	2	1406	3
Cross-links within Pro-σ^K									
Cross-linker	Peptide 1	Peptide 2	Residue 1	Residue 2	Score	Deviation (ppm)	Charge	Mass	Times Observed
DSS	NNAFPQPLSSSEE**K**	KYLELMA**K**GDEHAR	K38	K46	258	-1.82	4	3362	1
DSS	NNAFPQPLSSSEE**K**	KYLELMA**K**	K38	K46	66	-2.13	2	2680	1
DSS	NNAFPQPLSSSEE**KK**	YLELMA**K**GDEHAR	K38 or K39	K46	257	-1.82	4	3362	1
BS3	NNAFPQPLSSSEE**KK**	YLELMA**K**GDEHAR	K38 or K39	K46	89	-0.28	4	3346	2
DSS	NNAFPQPLSSSEE**KK**	YLELMA**K**	K38 or K39	K46	66	-2.13	2	2680	1
DTSSP	NNAFPQPLSSSEE**KK**	**K**FENTGEDAEDLISIGTIGLIK	K38 or K39	K69	146	-4.87	4	4212	1
DSS	NNAFPQPLSSSEE**KK**	GIESYSAG**K**GTK	K38 or K39	K99	458	-3.43	3	3010	1
BS3	NNAFPQPLSSSEE**KK**	GT**K**LATYAAR	K38 or K39	K102	534	-0.34	3	2864	9
DSS	NNAFPQPLSSSEE**KK**	GT**K**LATYAAR	K38 or K39	K102	126	-2.06	4	2864	1
Sulfo-SMCC	NNAFPQPLSSSEE**KK**	**C**IENEILMHLR	K38 or K39	C110	342	-2.17	3	3281	1
DSS	**K**FENTGEDAEDLISIGTIGLIK	GT**K**LATYAAR	K69	K102	306	-0.8	4	3552	3
BS3	**K**FENTGEDAEDLISIGTIGLIK	GT**K**LATYAAR	K69	K102	109	0.76	4	3552	1
Sulfo-SMCC	GIESYSAG**K**GTK	**C**IENEILMHLR	K99	C110	152	-1.31	4	2802	18
Sulfo-SMCC	GT**K**LATYAAR	**C**IENEILMHLR	K102	C110	140	-1.53	3	2656	8

[a]Cross-linker abbreviations: disuccinimidyl suberate, DSS; bis(sulfosuccinimidyl)suberate, BS3; *N*-(α-maleimidoacetoxy)succinimide ester, AMAS; sulfosuccinimidyl-4-(*N*-maleimidomethyl)cyclohexane-1-carboxylate, SMCC; 1,8-bismaleimidodiethyleneglycol, BM(PEG)$_2$; 3,3'-dithiobis(sulfosuccinimidylpropionate), DTSSP

[b]Cross-linked residues are bold underlined. In some cases, the mass spectrometry data did not allow a distinction to be made between adjacent or nearby residues participating in the cross-link.

[c]Maximum score observed for the cross-link. Scores are calculated by comparing the MS/MS-spectrum with theoretical fragment ions using StavroX software.

[d]Deviation of theoretical and measured mass.

[e]Charge of the precursor.
[f]Singly charged, monoisotopic mass of the precursor.
[g]This cross-link was observed using SpoIVFB with a Q201C substitution.
[h]This cross-link implied a constraint used to build initial models, but the models violated this constraint by large values, so this constraint was not used to build the reported model. We speculate that this cross-link occurred in unfolded SpoIVFB.

Table S2 Summary of Chemical Cross-links

Chemical cross-links between SpoIVFB and Pro-σ^K

SpoIVFB Residue	Pro-σ^K Residue	Highest Score[a]	Times Observed	Average Violation (Å)[b]
K59	K69	322	5	0.1
C201	K68 or K69	66	2	0
K217	K46	252	1	0.1
K217	K39	116	2	0
C246	K38	71	1	0
C246	K69	395	3	0.5
C246	K99	86	1	0
C246	K102	75	1	1.1
C246	C110	85	4	0

Cross-links within SpoIVFB

Residue 1	Residue 2	Highest Score	Times Observed	Average Violation (Å)
K154	C246	81	2	2.0[c]
K154	C201	21	1	1.2[d]
K217	K223	173	2	0[c]
K217	C246	86	3	0[c]
K217	K247	66	1	0.2[c]
K223	K243	86	3	1.6
K223	C246	733	11	0.2
K223	K258	331	3	0.2
K230	K234	66	1	0
K230	C246	139	3	0.6
K234	C246	129	4	0.8
C246	K254	277	9	0.6
C246	K258	220	4	1.3
C246	K275	91	4	0.4
K254	K258	66	3	0

Cross-links within Pro-σ^K

Residue 1	Residue 2	Highest Score	Times Observed	Average Violation (Å)
K38	K46	258	2	0
K38 or K39	K46	257	4	0
K38	K69	146	1	0
K38 or K39	K99	458	1	0.4
K39	K102	534	10	0
K38	C110	342	1	0
K69	K102	306	4	0.1
K99	C110	152	18	0
K102	C110	140	8	0.3

[a]Maximum score observed for the cross-link. Scores are calculated by comparing the MS/MS-spectrum with theoretical fragment ions using StavroX software.
[b]The distance between Cα atoms of cross-linked residues in the model (average of A, B, C, and D chains for SpoIVFB and average of X and Y chains for Pro-σ^K, unless noted otherwise) minus the theoretical maximum distance for the cross-linker, with negative values reported as 0.
[c]Since this restraint was applied only to the A and C chains, the average violation is reported only for those chains.
[d]Since this restraint was applied only to the B and D chains, the average violation is reported only for those chains.

Table S3 Cross-linking Restraints Used in Modeling and Violations of the SpoIVFB·Pro-σ^K Complex Model

Cross-links between SpoIVFB and Pro-σ^K

Residues[a]	Cross-linker[b]	Observed cross-link	Minimum distance restraint (Å)	Maximum distance restraint (Å)	K (kcal/mol/Å^2)	Distance in model (Å)	Violation (Å)[c]
PROA 44 - PROX 18	disulfide	weak	3	9	5	8.4	0
PROA 44 - PROX 19	disulfide		3	7	5	10.8	3.8
PROA 44 - PROX 20	disulfide		3	7	5	8.7	1.7
PROA 44 - PROX 22	disulfide		3	7	5	8.3	1.3
PROA 44 - PROX 23	disulfide		3	7	5	9.5	2.5
PROA 44 - PROX 24	disulfide		3	7	5	5.2	0
PROA 44 - PROX 25	disulfide		3	7	5	8.3	1.3
PROA 44 - PROX 27	disulfide	no	7	100	2	12.4	0
PROA 135 - PROX 20	disulfide		3	7	5	4.9	0
PROA 135 - PROX 21	disulfide		3	7	5	7.4	0.4
PROA 135 - PROX 22	disulfide		3	7	5	8.6	1.6
PROA 135 - PROX 24	disulfide		3	7	5	9.7	2.7
PROA 135 - PROX 18	disulfide	no	7	100	2	10.1	0
PROA 135 - PROX 19	disulfide	no	7	100	2	5	0
PROA 135 - PROX 25	disulfide	no	7	100	2	14.7	0
PROA 70 - PROX 18	disulfide		3	7	5	7.5	0.5
PROA 70 - PROX 19	disulfide		3	7	5	10.1	3.1
PROA 70 - PROX 20	disulfide		3	7	5	10.3	3.3
PROA 70 - PROX 21	disulfide		3	7	5	6.8	0
PROA 70 - PROX 22	disulfide		3	7	5	5.6	0
PROA 70 - PROX 23	disulfide		3	7	5	9	2
PROA 70 - PROX 24	disulfide		3	7	5	6	0
PROA 70 - PROX 25	disulfide		3	7	5	4.6	0
PROA 70 - PROX 27	disulfide		3	7	5	8.3	1.3
PROA 70 - PROX 29	disulfide	very weak	5	20	5	9.7	0
PROC 44 - PROY 18	disulfide	weak	3	9	5	9.4	0.4
PROC 44 - PROY 19	disulfide		3	7	5	9.1	2.1
PROC 44 - PROY 20	disulfide		3	7	5	8.8	1.8
PROC 44 - PROY 22	disulfide		3	7	5	4.8	0
PROC 44 - PROY 23	disulfide		3	7	5	8.8	1.8
PROC 44 - PROY 24	disulfide		3	7	5	9.6	2.6
PROC 44 - PROY 25	disulfide		3	7	5	7.5	0.5
PROC 44 - PROY 27	disulfide	no	7	100	2	10.8	0
PROC 135 - PROY 20	disulfide		3	7	5	4.9	0
PROC 135 - PROY 21	disulfide		3	7	5	9	2
PROC 135 - PROY 22	disulfide		3	7	5	8.4	1.4
PROC 135 - PROY 24	disulfide		3	7	5	11.7	4.7
PROC 135 - PROY 18	disulfide	no	7	100	2	9.7	0
PROC 135 - PROY 19	disulfide	no	7	100	2	6.7	0
PROC 135 - PROY 25	disulfide	no	7	100	2	14.2	0
PROC 70 - PROY 18	disulfide		3	7	5	10.4	3.4
PROC 70 - PROY 19	disulfide		3	7	5	8.7	1.7
PROC 70 - PROY 20	disulfide		3	7	5	11.5	4.5
PROC 70 - PROY 21	disulfide		3	7	5	9.1	2.1
PROC 70 - PROY 22	disulfide		3	7	5	4.7	0
PROC 70 - PROY 23	disulfide		3	7	5	8.3	1.3
PROC 70 - PROY 24	disulfide		3	7	5	7.7	0.7
PROC 70 - PROY 25	disulfide		3	7	5	5	0
PROC 70 - PROY 27	disulfide		3	7	5	7.6	0.6
PROC 70 - PROY 29	disulfide	very weak	5	20	5	12.1	0
PROA 59 - PROX 69	DSS/BS3		5	15	20	15.1	0.1
PROC 59 - PROY 69	DSS/BS3		5	15	20	14.7	0
PROA 201 - PROX 69	DSS/BS3		3	10	20	5.4	0

PROC 201 - PROY 69	DSS/BS3	3	10	20	10.1	0.1
PROA 201 - PROX 68	AMAS	3	10	20	9.6	0
PROC 201 - PROY 68	AMAS	3	10	20	5.4	0
PROA 217 - PROX 46	DSS	5	15	20	14.1	0
PROC 217 - PROY 46	DSS	5	15	20	15.1	0.1
PROA 217 - PROX 39	DSS	5	15	20	8.1	0
PROC 217 - PROY 39	DSS	5	15	20	5	0
PROA 246 - PROX 38[d]	SMCC	4	12	20	10.6	0
PROC 246 - PROY 38[d]	SMCC	4	12	20	7.6	0
PROA 246 - PROX 69	SMCC	4	12	20	12.9	0.9
PROC 246 - PROY 69	SMCC	4	12	20	11.7	0
PROA 246 - PROX 99	SMCC	4	12	20	7.4	0
PROC 246 - PROY 99	SMCC	4	12	20	9.7	0
PROA 246 - PROX 102	SMCC	4	12	20	14.2	2.2
PROC 246 - PROY 102	SMCC	4	12	20	11.8	0
PROA 246 - PROX 110	BM(PEG)2	7	20	20	11.9	0
PROC 246 - PROY 110	BM(PEG)2	7	20	20	16.2	0

Cross-links within SpoIVFB

Residues	Cross-linker	Observed cross-link	Minimum distance restraint (Å)	Maximum distance restraint (Å)	K (kcal/mol/Å^2)	Distance in model (Å)	Violation (Å)
PROA 154 - PROA 246	SMCC		4	12	20	14.4	2.4
PROC 154 - PROC 246	SMCC		4	12	20	13.5	1.5
PROB 201 - PROB 154	AMAS		3	10	20	11.8	1.8
PROD 201 - PROD 154	AMAS		3	10	20	10.5	0.5
PROA 217 - PROA 223	DSS		5	15	20	6.3	0
PROC 217 - PROC 223	DSS		5	15	20	6.8	0
PROA 217 - PROA 246	SMCC		4	12	20	5.8	0
PROC 217 - PROC 246	SMCC		4	12	20	9.1	0
PROA 217 - PROA 247	BS3		5	15	20	12	0
PROC 217 - PROC 247	BS3		5	15	20	15.3	0.3
PROA 223 - PROA 243	DSS		5	15	20	15.1	0.1
PROB 223 - PROB 243	DSS		5	15	20	16.8	1.8
PROC 223 - PROC 243	DSS		5	15	20	15.5	0.5
PROD 223 - PROD 243	DSS		5	15	20	19	4
PROA 223 - PROA 246	SMCC		4	12	20	9.1	0
PROB 223 - PROB 246	SMCC		4	12	20	12.2	0.2
PROC 223 - PROC 246	SMCC		4	12	20	7.7	0
PROD 223 - PROD 246	SMCC		4	12	20	12.6	0.6
PROA 223 - PROA 258	DSS		5	15	20	15.4	0.4
PROB 223 - PROB 258	DSS		5	15	20	11.4	0
PROC 223 - PROC 258	DSS		5	15	20	15.4	0.4
PROD 223 - PROD 258	DSS		5	15	20	8	0
PROA 230 - PROA 234	BS3		5	15	20	11.9	0
PROB 230 - PROB 234	BS3		5	15	20	6.9	0
PROC 230 - PROC 234	BS3		5	15	20	12.5	0
PROD 230 - PROD 234	BS3		5	15	20	6.1	0
PROA 230 - PROA 246	SMCC		4	12	20	13.4	1.4
PROB 230 - PROB 246	SMCC		4	12	20	9.9	0
PROC 230 - PROC 246	SMCC		4	12	20	13	1
PROD 230 - PROD 246	SMCC		4	12	20	12.1	0.1
PROA 234 - PROA 246	SMCC		4	12	20	11.7	0
PROB 234 - PROB 246	SMCC		4	12	20	12.2	0.2
PROC 234 - PROC 246	SMCC		4	12	20	13.4	1.4
PROD 234 - PROD 246	SMCC		4	12	20	13.5	1.5
PROA 246 - PROA 254[e]	SMCC		4	12	20	7.8	0
PROB 246 - PROB 254[e]	SMCC		4	12	20	13.2	1.2

PROC 246 - PROC 254[e]	SMCC	4	12	20	8.5	0
PROD 246 - PROD 254[e]	SMCC	4	12	20	13	1
PROA 246 - PROA 258	SMCC	4	12	20	13.8	1.8
PROB 246 - PROB 258	SMCC	4	12	20	12.9	0.9
PROC 246 - PROC 258	SMCC	4	12	20	14.2	2.2
PROD 246 - PROD 258	SMCC	4	12	20	12.2	0.2
PROA 246 - PROA 275	SMCC	4	12	20	12.8	0.8
PROB 246 - PROB 275	SMCC	4	12	20	9.9	0
PROC 246 - PROC 275	SMCC	4	12	20	12.9	0.9
PROD 246 - PROD 275	SMCC	4	12	20	10.5	0
PROA 254 - PROA 258	BS3	5	15	20	6.8	0
PROB 254 - PROB 258	BS3	5	15	20	12.2	0
PROC 254 - PROC 258	BS3	5	15	20	6.8	0
PROD 254 - PROD 258	BS3	5	15	20	11.2	0

Cross-links within Pro-σ^K

Residues	Cross-linker	Observed cross-link	Minimum distance restraint (Å)	Maximum distance restraint (Å)	K (kcal/mol/Å^2)	Distance in model (Å)	Violation (Å)
PROX 38 - PROX 46	DSS/BS3		5	15	20	5.8	0
PROY 38 - PROY 46	DSS/BS3		5	15	20	14	0
PROX 39 - PROX 46	DSS/BS3		5	15	20	9.9	0
PROY 39 - PROY 46	DSS/BS3		5	15	20	10.8	0
PROX 38 - PROX 69[f]	DTSSP		5	16	20	15.2	0
PROY 38 - PROY 69[f]	DTSSP		5	16	20	10.9	0
PROX 38 - PROX 99	DSS		5	15	20	12.9	0
PROY 38 - PROY 99	DSS		5	15	20	6.7	0
PROX 39 - PROX 99	DSS		5	15	20	16.5	1.5
PROY 39 - PROY 99	DSS		5	15	20	15.1	0.1
PROX 38 - PROX 110[f]	SMCC		4	12	20	9.8	0
PROY 38 - PROY 110[f]	SMCC		4	12	20	8.7	0
PROX 39 - PROX 102[g]	DSS/BS3		5	15	20	11.5	0
PROY 39 - PROY 102[g]	DSS/BS3		5	15	20	14	0
PROX 69 - PROX 102	DSS/BS3		5	15	20	8.3	0
PROY 69 - PROY 102	DSS/BS3		5	15	20	4.8	0.2
PROX 99 - PROX 110	SMCC		4	12	20	8.1	0
PROY 99 - PROY 110	SMCC		4	12	20	10.5	0
PROX 102 - PROX 110	SMCC		4	12	20	12	0
PROY 102 - PROY 110	SMCC		4	12	20	12.5	0.5

[a]The chain and residue of protein (PRO) SpoIVFB is listed first, followed by the chain and residue of Pro-σ^K.

[b]Abbreviations of chemical cross-linkers are listed in Table S1 footnote [a].

[c]The distance between Cα atoms of cross-linked residues in the model minus the theoretical maximum distance for the cross-linker, with negative values reported as 0.

[d]The cross-linking did not distinguish between residues 38 and 39 of Pro-σ^K (Table S1), so both were used in the initial round of modeling, but residue 39 was omitted in the final round of modeling because it resulted in slightly higher violations.

[e]The cross-linking did not distinguish between residues 254 and 258 of SpoIVFB (Table S1), so both were used in the initial round of modeling, but residue 258 was omitted in the final round of modeling because it resulted in slightly higher violations.

[f]The cross-linking did not distinguish between residues 38 and 39 of Pro-σ^K (Table S1), so both were used in the initial round of modeling, but residue 39 was omitted in the final round of modeling because it resulted in slightly higher violations.

[g]The cross-linking did not distinguish between residues 38 and 39 of Pro-σ^K (Table S1), so both were used in the initial round of modeling, but residue 38 was omitted in the final round of modeling because it resulted in slightly higher violations.

Table S4. Plasmids used in this study

Plasmid	Description[a, b]	Construction	Reference
pDP40	Sp^R; *amyE*::*spoIVF* with SpoIVFB H206A	pDR18a was subjected to site-directed mutagenesis using primers SH29 and SH30	This study
pDP41	Sp^R; *amyE*::*spoIVF* with SpoIVFB F209A	pDR18a was subjected to site-directed mutagenesis using primers SH35 and SH36	This study
pDP42	Sp^R; *amyE*::*spoIVF* with SpoIVFB R213A	pDR18a was subjected to site-directed mutagenesis using primers SH37 and SH38	This study
pDP43	Sp^R; *amyE*::*spoIVF* with SpoIVFB H206A F209A R213A	pDR18a was subjected to site-directed mutagenesis using primers SH61 and SH62	This study
pDP61	Sp^R; *amyE*::*spoIVF* with SpoIVFB H206F	pDR18a was subjected to site-directed mutagenesis using primers DP127 and DP128	This study
pDP62	Sp^R; *amyE*::*spoIVF* with SpoIVFB R208Q	pDR18a was subjected to site-directed mutagenesis using primers DP135 and DP136	This study
pDP63	Sp^R; *amyE*::*spoIVF* with SpoIVFB F209D	pDR18a was subjected to site-directed mutagnesis using primers DP129 and DP130	This study
pDP64	Sp^R; *amyE*::*spoIVF* with SpoIVFB L210I	pDR18a was subjected to site-directed mutagenesis using primers DP137 and DP138	This study
pDP65	Sp^R; *amyE*::*spoIVF* with SpoIVFB R213K	pDR18a was subjected to site-directed mutagenesis using primers DP131 and DP132	This study
pDP74	Ap^R; TM-SpoIVFB-F2-H2 R208A	pZR209 was subjected to site-directed mutagenesis using primers SH33 and SH34	This study
pDP75	Ap^R; TM-SpoIVFB-F2-H2 F209A	pZR209 was subjected to site-directed mutagenesis using primers SH35 and SH36	This study
pDR18a	Sp^R; *amyE*::*spoIVF*	The intact *spoIVF* operon was cloned into pLD30	(13)
pSH01	Ap^R; TM-SpoIVFB(1-197)-F2	SpoIVFB(1-197) was amplified by PCR using pZR209 as template and primers LK1385 and SH92, the fragment was digested with BamHI and HindIII, and ligated to BamHI-HindIII-digested pYZ68	This study
pSH02	Ap^R; TM-SpoIVFB(1-222)-F2	SpoIVFB(1-222) was amplified by PCR using pZR209 as template and primers LK1385 and SH91, the fragment was digested with BamHI and HindIII, and ligated to BamHI-HindIII-digested pYZ68	This study
pSH03	Ap^R; TM-SpoIVFB(212-288)-F2	SpoIVFB(212-288) was amplified by PCR using pZR209 as template and primers SH89 and SH84, the fragment was digested with BamHI and HindIII, and ligated to BamHI-HindIII-digested pYZ68	This study
pSH04	Ap^R; TM-SpoIVFB(222-288)-F2	SpoIVFB(222-288) was amplified by PCR using pZR209 as template and primers SH88 and SH84, the fragment was digested with BamHI and HindIII, and ligated to BamHI-HindIII-digested pYZ68	This study
pSH05	Ap^R; TM-SpoIVFB(197-288)-F2	SpoIVFB(197-288) was amplified by PCR using pZR209 as template and primers SH83 and SH84, the fragment was digested with BamHI and HindIII, and ligated to BamHI-HindIII-digested pYZ68	This study
pSH06	Ap^R; TM-SpoIVFB(197-222)-F2	SpoIVFB(197-222) was amplified by PCR using pZR209 as template and primers SH83 and SH91, the fragment was digested with	This study

		BamHI and HindIII, and ligated to BamHI-HindIII-digested pYZ68	
pSH07	Ap^R; TM-SpoIVFB(1-212)-F2	SpoIVFB(1-212) was amplified by PCR using pZR209 as template and primers LK1385 and SH90, the fragment was digested with BamHI and HindIII, and ligated to BamHI-HindIII-digested pYZ68	This study
pSH08	Ap^R; TM-SpoIVFB(EYR198-200AAA)-F2-H2	pZR209 was subjected to site-directed mutagenesis using primers SH01 and SH02	This study
pSH09	Ap^R; TM-SpoIVFB(QRH201-203AAA)-F2-H2	pZR209 was subjected to site-directed mutagenesis using primers SH03 and SH04	This study
pSH10	Ap^R; TM-SpoIVFB(YIH204-206AAA)-F2-H2	pZR209 was subjected to site-directed mutagenesis using primers SH05 and SH06	This study
pSH11	Ap^R; TM-SpoIVFB(VRF207-209AAA)-F2-H2	pZR209 was subjected to site-directed mutagenesis using primers SH07 and SH08	This study
pSH12	Ap^R; TM-SpoIVFB(LLE210-212AAA)-F2-H2	pZR209 was subjected to site-directed mutagenesis using primers SH09 and SH10	This study
pSH13	Ap^R; TM-SpoIVFB(RYY213-215AAA)-F2-H2	pZR209 was subjected to site-directed mutagenesis using primers SH11 and SH12	This study
pSH14	Ap^R; TM-SpoIVFB(GKN216-218AAA)-F2-H2	pZR209 was subjected to site-directed mutagenesis using primers SH13 and SH14	This study
pSH15	Ap^R; TM-SpoIVFB(REL219-221AAA)-F2-H2	pZR209 was subjected to site-directed mutagenesis using primers SH15 and SH16	This study
pSH16	Ap^R; TM-SpoIVFB(EKL222-224AAA)-F2-H2	pZR209 was subjected to site-directed mutagenesis using primers SH17 and SH18	This study
pSH26	Ap^R; TM-SpoIVFB-F2-H2 with residues 201-212 changed to alanine	pZR209 was subjected to site-directed mutagenesis using primers SH55 and SH56	This study
pSH27	Ap^R; TM-SpoIVFB-F2 with residues 201-212 changed to alanine	pYZ68 was subjected to site-directed mutagenesis using primers SH55 and SH56	This study
pSH28	Ap^R; TM-SpoIVFB-F2-H2 E198A	pZR209 was subjected to site-directed mutagenesis using primers SH19 and SH20	This study
pSH30	Ap^R; TM-SpoIVFB-F2-H2 Y199A	pZR209 was subjected to site-directed mutagenesis using primers SH21 and SH22	This study
pSH31	Ap^R; TM-SpoIVFB-F2-H2 R200A	pZR209 was subjected to site-directed mutagenesis using primers SH23 and SH24	This study
pSH36	Ap^R; TM-SpoIVFB-F2-H2 Y204A	pZR209 was subjected to site-directed mutagenesis using primers SH25 and SH26	This study
pSH38	Ap^R; TM-SpoIVFB-F2-H2 I205A	pZR209 was subjected to site-directed mutagenesis using primers SH27 and SH28	This study
pSH39	Ap^R; TM-SpoIVFB-F2-H2 H206A	pZR209 was subjected to site-directed mutagenesis using primers SH29 and SH30	This study
pSH41	Ap^R; TM-SpoIVFB-F2-H2 V207A	pZR209 was subjected to site-directed mutagenesis using primers SH31 and SH32	This study
pSH43	Ap^R; TM-SpoIVFB-F2-H2 R213A	pZR209 was subjected to site-directed mutagenesis using primers SH37 and SH38	This study
pSH45	Ap^R; TM-SpoIVFB-F2-H2 Y214A	pZR209 was subjected to site-directed mutagenesis using primers SH39 and SH40	This study
pSH48	Ap^R; TM-SpoIVFB-F2-H2 Y215A	pZR209 was subjected to site-directed mutagenesis using primers SH41 and SH42	This study
pSH49	Ap^R; TM-SpoIVFB-F2-H2 G216A	pZR209 was subjected to site-directed mutagenesis using primers SH43 and SH44	This study
pSH52	Ap^R; TM-SpoIVFB-F2-H2 K217A	pZR209 was subjected to site-directed mutagenesis using primers SH45 and SH46	This study

pSH54	Ap^R; TM-SpoIVFB-F2-H2 N218A	pZR209 was subjected to site-directed mutagenesis using primers SH47 and SH48	This study
pSH55	Ap^R; TM-SpoIVFB-F2 E44Q H206A	pYZ68 was subjected to site-directed mutagenesis using primers SH29 and SH30	This study
pSH56	Ap^R; TM-SpoIVFB-F2 E44Q F209A	pYZ68 was subjected to site-directed mutagenesis using primers SH35 and SH36	This study
pSH57	Ap^R; TM-SpoIVFB-F2 E44Q R213A	pYZ68 was subjected to site-directed mutagenesis using primers SH37 and SH38	This study
pSH58	Ap^R; TM-SpoIVFB-F2 E44Q H206A F209A R213A	pYZ68 was subjected to site-directed mutagenesis using primers SH61 and SH62	This study
pSH59	Km^R; Pro-σ^K(1-127)-H6/ SpoIVFB-TEV-F2 E44Q Q201C	pYZ42 was subjected to site-directed mutagenesis using primers SH65 and SH66	This study
pYZ42	Km^R; Pro-σ^K(1-126)-H6/ SpoIVFB-TEV-F2 E44Q		(2)
pYZ68	Ap^R; TM-SpoIVFB-F2 E44Q		(2)
pZR12	Km^R; Pro-σ^K(1-127)-H6		(15)
pZR209	Ap^R; TM-SpoIVFB-F2-H6		(1)

[a]Abbreviations: Sp^R, spectinomycin-resistant; Ap^R, ampicillin-resistant; TM, transmembrane segment from rabbit Cytochrome P450 2B4; F2, two FLAG epitopes; H6, 6 His residues; Km^R, kanamycin-resistant; TEV, Tobacco Etch Virus protease cleavage site.
[b]Each protein listed is preceded by a T7 RNA polymerase promoter and a translation initiation sequence to permit expression in *E. coli*.

Table S5. Primers used in this study

Primer	Sequence
DP127	CGGCAAAGGCACTATATCTTTGTGAGATTTCTCCTCGAA
DP128	TTCGAGGAGAAATCTCACAAAGATATAGTGCCTTTGCCG
DP129	CACTATATCCATGTGAGAGATCTCCTCGAAAGGTATTAC
DP130	GTAATACCTTTCGAGGAGATCTCTCACATGGATATAGTG
DP131	GTGAGATTTCTCCTCGAAAAGTATTACGGAAAAAACAGG
DP132	CCTGTTTTTTCCGTAATACTTTTCGAGGAGAAATCTCAC
DP135	AGGCACTATATCCATGTGCAATTTCTCCTCGAAAGGTAT
DP136	ATACCTTTCGAGGAGAAATTGCACATGGATATAGTGCCT
DP137	TATATCCATGTGAGATTTATCCTCGAAAGGTATTACGGA
DP138	TCCGTAATACCTTTCGAGGATAAATCTCACATGGATATA
LK1385	CGGGATCCATGAATAAATGGCTCGACCTTATC
SH01	GTTTCCTTGTTTGAGGCAGCGGCACAAAGGCACTATATC
SH02	GATATAGTGCTCTTGTGCCGCTGCCTCAAACAAGGAAAC
SH03	GTTTGAGGAATATCGGGCAGCGGCATATATCATGTGAG
SH04	CTCACATGGATATATGCCGCTGCCCGATATTCCTCAAAC
SH05	GAATATCGGCAAAGGCACGCAGCGGCAGTGAGATTTCTCCTC
SH06	GAGGAGAAATCTCACTGCCGCTGCGTGCCTTTGCCGATATTC
SH07	GGCACTATATCCATGCAGCGGCACTCCTCGAAAGGKTATTAC
SH08	GTAATACCTTTCGAGGAGTGCCGCTGCATGGATATAGTGCC
SH09	CTATATCCATGTGAGATTTGCAGCGGCAAGGTATTACGGAAAAAAC
SH10	GTTTTTTCCGTAATACCTTGCCGCTGCAAATCTCACATGGATATAG
SH11	GAGATTTCTCCTCGAAGCAGCGGCAGGAAAAAACAGGGAG
SH12	CTCCCTGTTTTTTCCTGCCGCTGCTTCGAGGAGAAATCTC
SH13	CTCGAAAGGTATTACGCAGCGGCAAGGGAGCTTGAGCTTGAGAAACTTC
SH14	GAAGTTTCTCAAGCTCCCTTGCCGCTGCGTAATACCTTTCG AG
SH15	GTATTACGGAAAAAACAGGGCAGCGGCAAAACTTCTGCTGCCGCTGAC
SH16	GTCAGCGGCAGAAGTTTTGCCGCTGCCCTGTTTTTTCCGTAATAC
SH17	GAAAAAACAGGGAGCTTGAGGCAGCGGCACCGCCGCTGACAGTAAAG
SH18	CTTTACTGTCAGCGTGCCGCTGCCTCAAGCTCCCTGTTTTTTC
SH19	GTTTCCTTGTTTGAGGCATATCGGCAAAGGCAC
SH20	GTGCCTTTGCCGATATGCCTCAAACAAGGAAAC
SH21	GTTTCCTTGTTTGAGGAAGCACGGCAAAGGCACTATATC
SH22	GATATAGTGCCTTTGCCGTGCTTCCTCAAACAAGGAAAC
SH23	GTTTCCTTGTTTGAGGAATATGCGCAAAGGCACTATATCCATG
SH24	CATGGATATAGTGCCTTTGCGCATATTCCTCAAACAAGGAAAC
SH25	GAATATCGGCAAAGGCACGCAATCCATGTGAGATTTCTC
SH26	GAGAAATCTCACATGGATTGCGTGCCTTTGCCGATATTC
SH27	CGGCAAAGGCACTATGCGCATGTGAGATTTCTCCTC
SH28	GAGGAGAAATCTCACATGCGCATAGTGCCTTTGCCG
SH29	GGCAAAGGCACTATATCGCGGTGAGATTTCTCCTCG
SH30	CGAGGAGAAATCTCACCGCGATATAGTGCCTTTGCC
SH31	GGCACTATATCCATGCGAGATTTCTCCTCG
SH32	CGAGGAGAAATCTCGCATGGATATAGTGCC
SH33	GGCACTATATCCATGTGGCATTTCTCCTCGAAAGG
SH34	CCTTTCGAGGAGAAATGCCACATGGATATAGTGCC
SH35	CACTATATCCATGTGAGAGCACTCCTCGAAAGGTATTACG
SH36	CGTAATACCTTTCGAGGAGTGCTCTCACATGGATATAGTG
SH37	GTGAGATTTCTCCTCGAAGCGTATTACGGAAAAAACAG
SH38	CTGTTTTTTCCGTAATACGCTTCGAGGAGAAATCTCAC
SH39	GATTTCTCCTCGAAAGGGCATACGGAAAAAACAGGGAG

SH40	CTCCCTGTTTTTTCCGTATGCCCTTTCGAGGAGAAATC
SH41	GATTTCTCCTCGAAAGGTATGCGGGAAAAAACAGGGAGCTTG
SH42	CAAGCTCCCTGTTTTTTCCCGCATACCTTTCGAGGAGAAATC
SH43	CTCGAAAGGTATTACGCAAAAAACAGGGAGCTTG
SH44	CAAGCTCCCTGTTTTTTGCGTAATACCTTTCGAG
SH45	CGAAAGGTATTACGGAGCAAACAGGGAGCTTGAG
SH46	CTCAAGCTCCCTGTTTGCTCCGTAATACCTTTCG
SH47	GAAAGGTATTACGGAAAAGCGAGGGAGCTTGAGAAACTTC
SH48	GAAGTTTCTCAAGCTCCCTCGCTTTTCCGTAATACCTTTC
SH55	GTTTCCTTGTTTGAGGAATATCGGGCAGCGGCAGCGGCAGCGGCAGCGGCAGCGGCA GCGAGGTATTACGGAAAAAAC
SH56	GTTTTTTCCGTAATACCTCGCTGCCGCTGCCGCTGCCGCTGCCGCTGCCGCTGC CCGATATTCCTCAAACAAGGAAAC
SH61	GGCAAAGGCACTATATCGCGGTGAGAGCACTCCTCGAAGCGTATTACGGAAAAAACAG
SH62	CTGTTTTTTCCGTAATACGCTTCGAGGAGTGCTCTCACCGCGATATAGTGCCTTTGCC
SH65	GTTTCCTTGTTTGAGGAATATCGGTGTAGGCACTATATCCATGTGAG
SH66	CTCACATGGATATAGTGCCTACACCGATATTCCTCAAACAAGGAAAC
SH83	CGGGATCCGAATATCGGCAAAGGCAC
SH84	GCCAAGCTTGTAGGGCAGAAGCAGTTCC
SH88	CGGGATCCTTCGAGGAGAAATCTCACAT
SH89	CGGGATCCGAAAGGTATTACGGAAAAAACAGG
SH90	GCCAAGCTTTTCGAGGAGAAATCTCACAT
SH91	GCCAAGCTTCTCAAGCTCCCTGTTTTTTC
SH92	GCCAAGCTTCTCAAACAAGGAAACAGCCAG

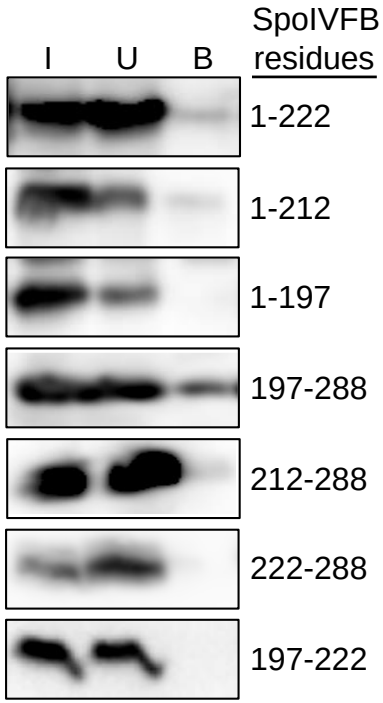

Figure S1. Control pull-down assays of SpoIVFB derivatives in the absence of Pro-σ^K. The indicated deletion derivative was expressed without Pro-σ^K in *E. coli* for 2 h and samples were subjected to pull-down assays. Input (I), unbound (U), and bound (B) fractions were subjected to immunoblot analysis with anti-FLAG antibodies. More of the 197-288 derivative was bound in the absence of Pro-σ^K than for the other derivatives. Neverthless, more of the 197-288 was bound in the presence of Pro-σ^K (Fig. 1C) than in its absence.

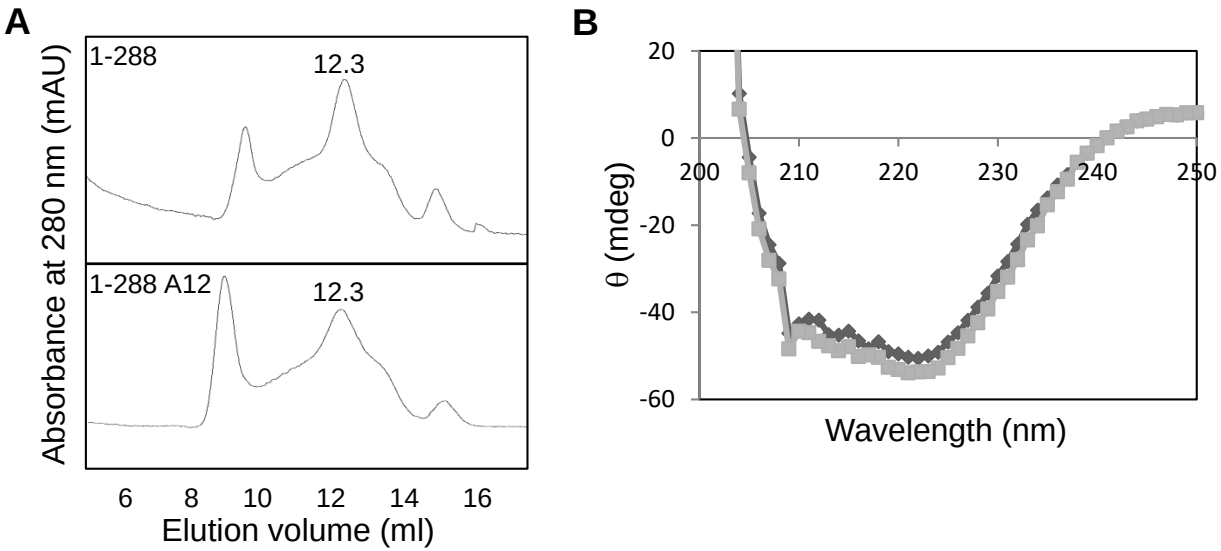

Figure S2. Purification of SpoIVFB. (A) Size exclusion chromatography during purification of SpoIVFB 1-288 (top) and 1-288 A12 (bottom). Proteins expressed in *E. coli* were subjected to cobalt-affinity purification, the bound fraction was concentrated and applied to a size exclusion column, and the absorbance at 280 nm was monitored during elution to generate the profiles shown. The absorbance peak at 12.3 ml contains primarily SpoIVFB as judged by SDS-PAGE followed by Coomassie Blue staining. (B) Circular dichroism (CD) spectra of purified 1-288 (dark gray diamonds) and 1-288 A12 (light gray squares). CD at the indicated wavelengths was measured for protein samples that eluted from the size exclusion column in the fraction containing the absorbance peak at 12.3 ml in panel A.

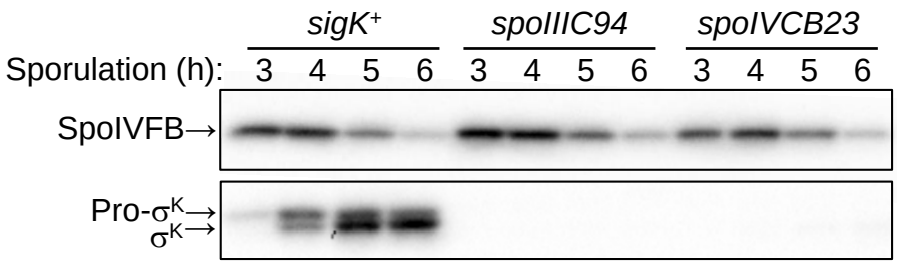

Figure S3. Effects of *sigK* mutations on SpoIVFB during *B. subtilis* sporulation. *B. subtilis* strain PY79 with a wild-type *sigK* gene or a mutation in the 3' (*spoIIIC94*) or 5' (*spoIVCB23*) half of *sigK* [strains BK410 (16) and BK556 (17), respectively], were induced to sporulate, and samples collected at the indicated times post-induction were subjected to immunoblot analysis with antibodies against SpoIVFB (top) or Pro-σ^K (bottom).

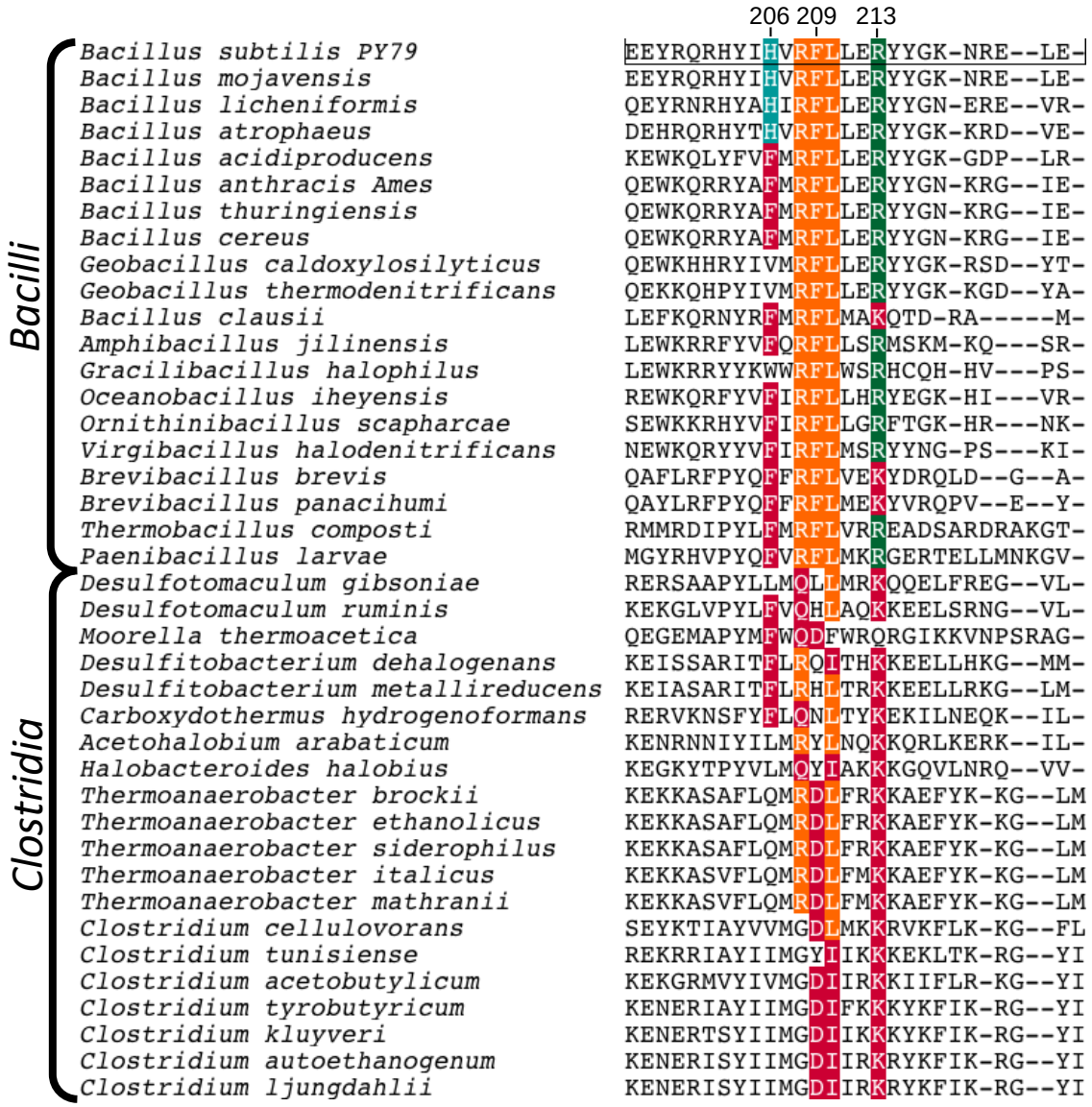

Figure S4. Alignment of SpoIVFB interdomain linker sequences. Representative sequences of *Bacilli* and *Clostridia* are shown from among 136 SpoIVFB orthologs. The *B. subtilis* sequence is boxed at the top with key residues numbered. Colors indicate conservation among sequences of 76 *Bacilli* (orange ≥90%, green ≥80%, teal ≤50%) or alternate conserved residues that guided substitutions made in *B. subtilis* SpoIVFB (red).

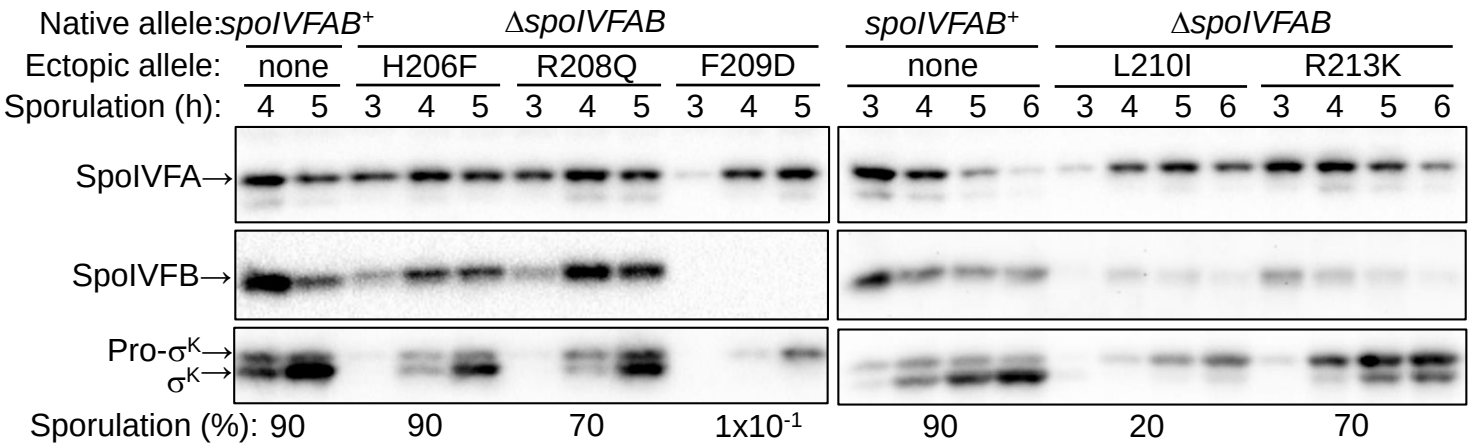

Figure S5. Effect of substitutions in the SpoIVFB interdomain linker during *B. subtilis* sporulation. The experiment was performed as described in the Figure 3 legend.

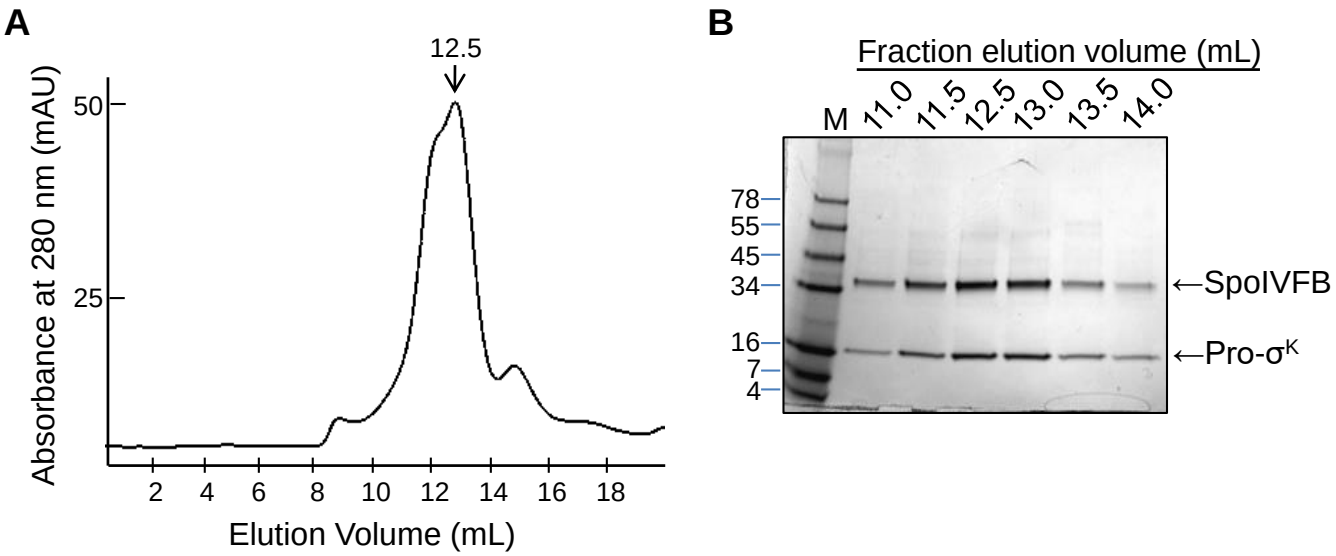

Figure S6. Purification of a SpoIVFB·Pro-σ^K complex. (A) Size exclusion chromatography UV absorbance profile. Pro-σ^K(1-127)-His_6 and SpoIVFB-TEV-$FLAG_2$ E44Q were coexpressed in *E. coli*, subjected to cobalt-affinity purification, the bound fraction was concentrated and applied to a size exclusion column, and the absorbance at 280 nm was monitored during elution, resulting in a broad peak with a maximum at 12.5 mL. (B) SDS/PAGE of fractions from the size exclusion column. Fractions eluting at the indicated volumes were subjected to SDS/PAGE followed by Coomassie Blue staining. Peak fractions contained predominantly SpoIVFB and Pro-σ^K as judged by migration versus protein markers (M, molecular weight in kDa at left) and immunoblot (e.g., Fig. 4B, lanes NC).

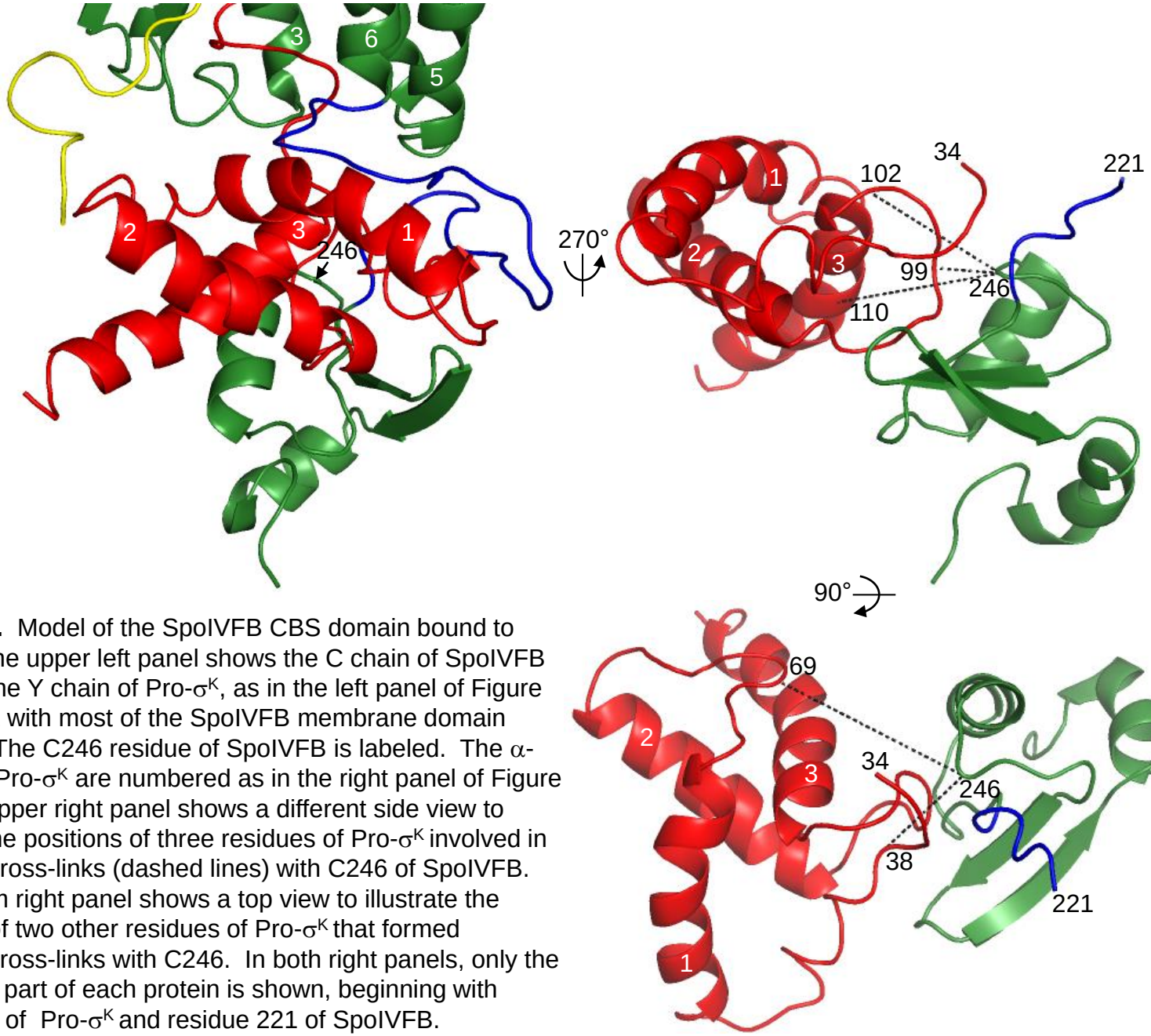

Figure S7. Model of the SpoIVFB CBS domain bound to Pro-σ^K. The upper left panel shows the C chain of SpoIVFB bound to the Y chain of Pro-σ^K, as in the left panel of Figure 5B, except with most of the SpoIVFB membrane domain cropped. The C246 residue of SpoIVFB is labeled. The α-helices of Pro-σ^K are numbered as in the right panel of Figure 5B. The upper right panel shows a different side view to illustrate the positions of three residues of Pro-σ^K involved in chemical cross-links (dashed lines) with C246 of SpoIVFB. The bottom right panel shows a top view to illustrate the positions of two other residues of Pro-σ^K that formed chemical cross-links with C246. In both right panels, only the C-terminal part of each protein is shown, beginning with residue 34 of Pro-σ^K and residue 221 of SpoIVFB.

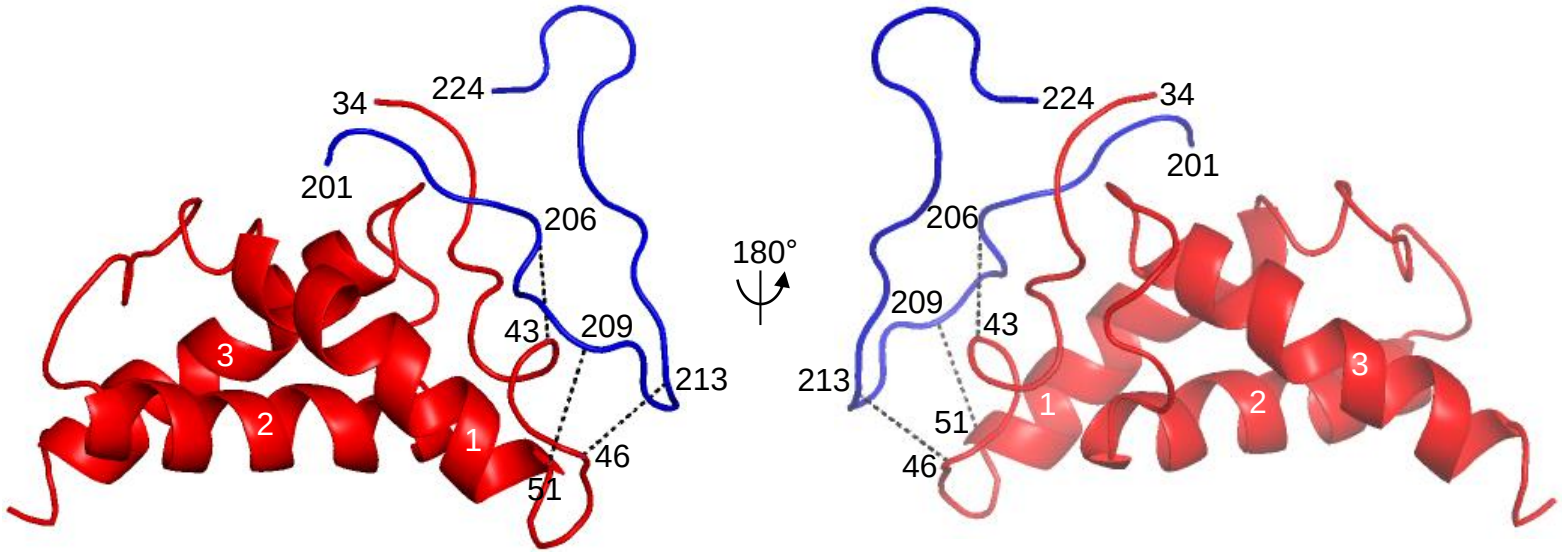

Figure S8. Model of the interaction between the SpoIVFB interdomain linker and residues 43-51 of Pro-σ^K. The left panel shows the Y chain of Pro-σ^K residues 34-122 in a similar orientation as in the right panel of Figure 5B, except rotated forward slightly. Only residues 201-224 of the C chain of the SpoIVFB linker are shown. Dashed lines indicate points of closest proximity (7 Å in each case) between the chains (distance between Cα atoms of indicated residues). The right panel shows the back view.

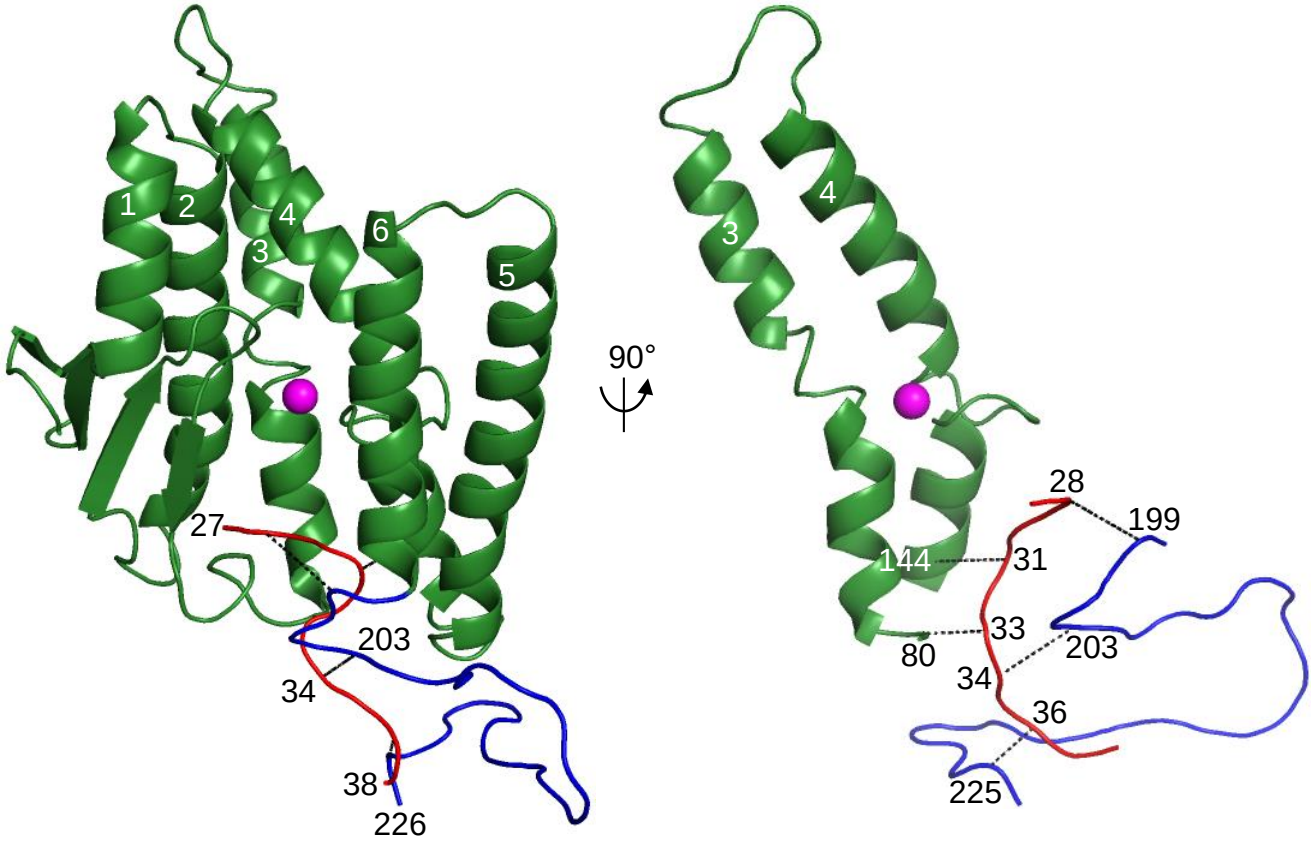

Figure S9. Model of the interaction between SpoIVFB and residues 28-36 of Pro-σ^K. The left panel shows the C chain of SpoIVFB residues 1-226 in a similar orientation as in the left panel of Figure 5B. Only residues 27-38 of the Y chain of Pro-σ^K are shown. Dashed lines indicate points of closest proximity (5-7 Å in each case) between the chains (distance between Cα atoms of indicated residues). The right panel shows a different side view, with residues 1-78 and 147-197 of SpoIVFB removed to better show the points of closest proximity.

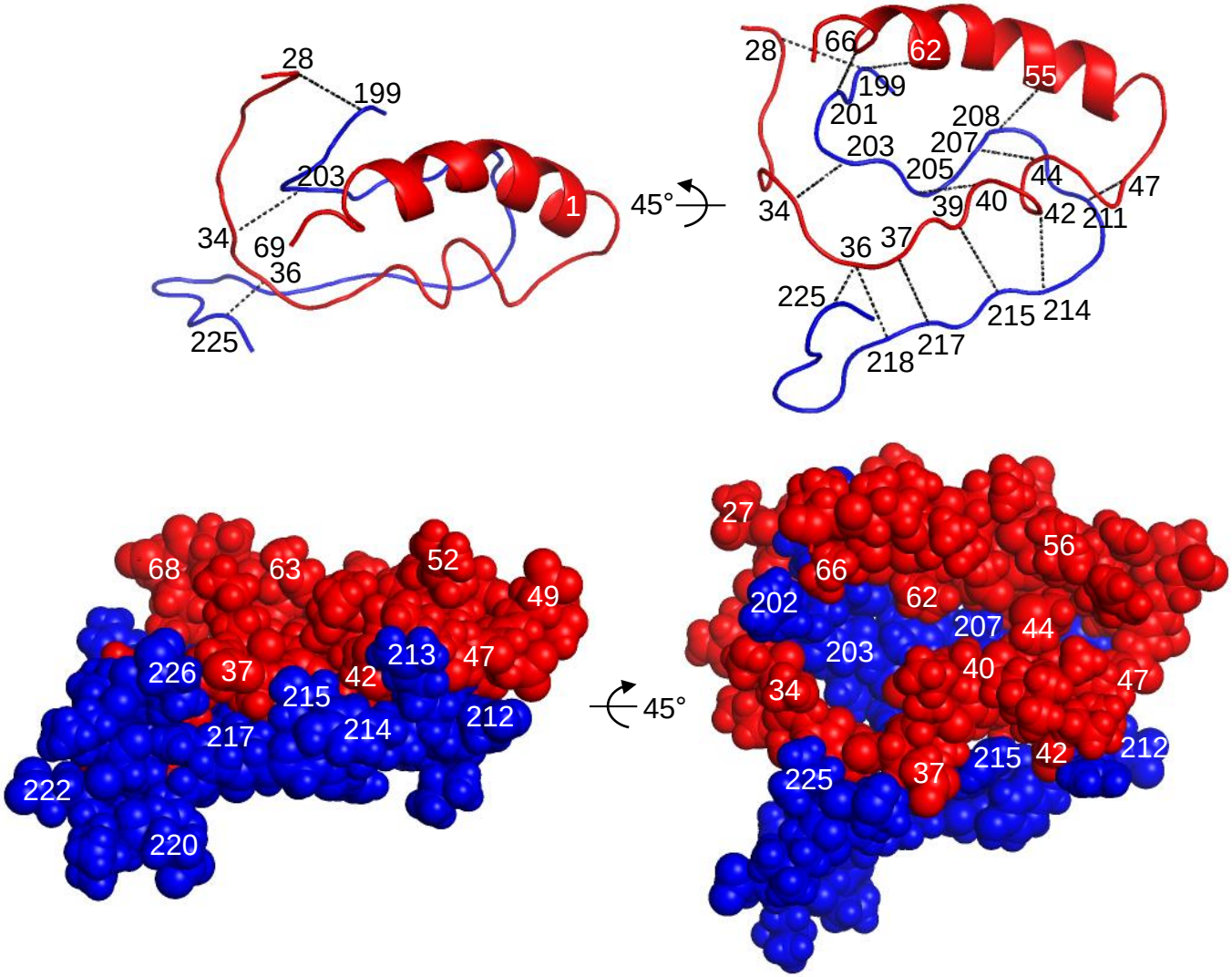

Figure S10. Model of the interaction between the SpoIVFB interdomain linker and residues 28-69 of Pro-σ^K. The upper left panel shows the C chain of SpoIVFB residues 198-226 as in the right panel of Figure S9. Residues 27-69 of the Y chain of Pro-σ^K are shown, with α-helix 1 labeled. Dashed lines indicate points of proximity (5-7 Å in each case) between the chains (distance between Cα atoms of indicated residues). The upper right panel shows additional points of proximity (6-8 Å in each case). The lower right panel shows the same view with side chains added and space-filling atoms to illustrate packing. The lower left panel further illustrates packing.

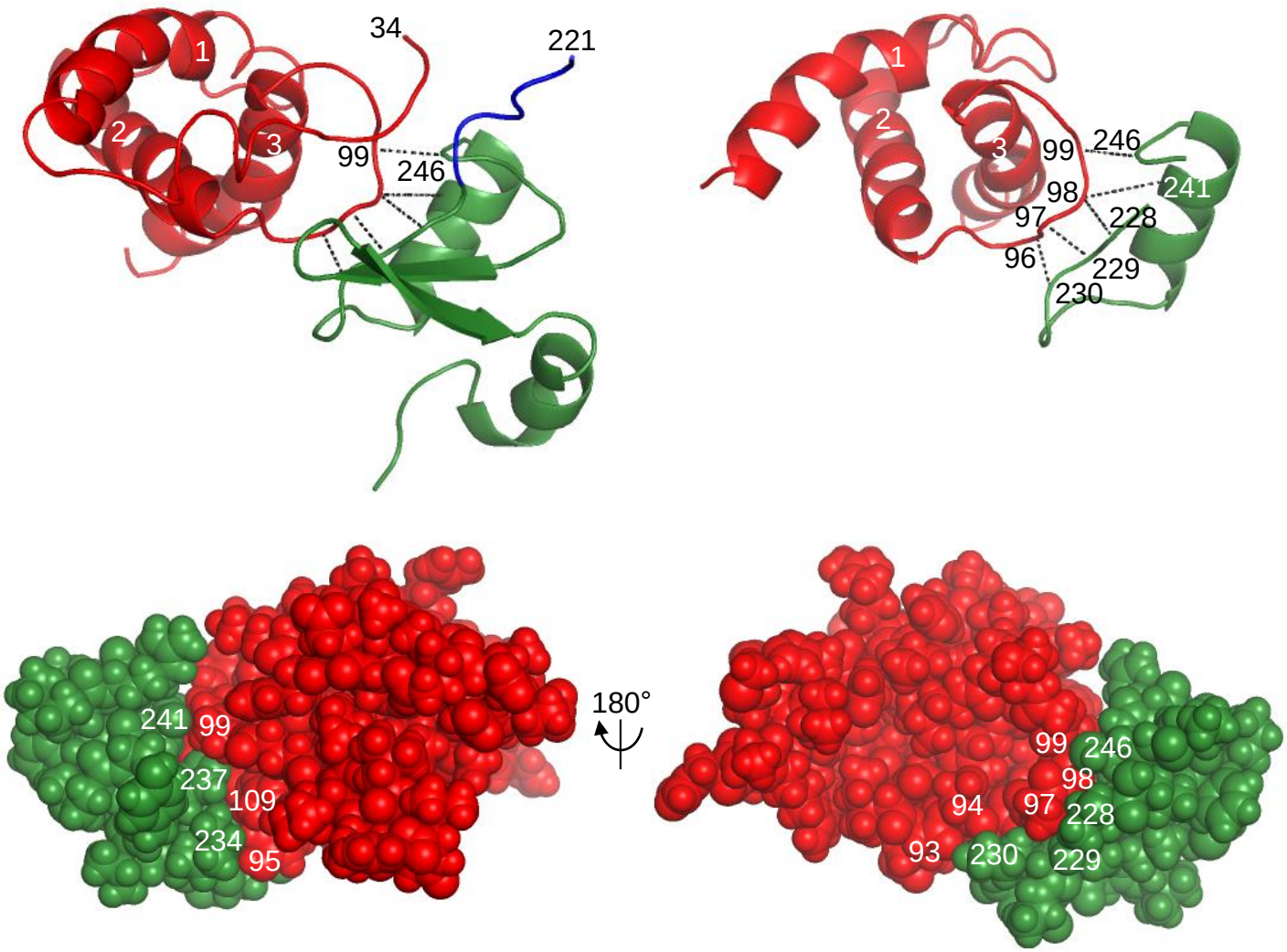

Figure S11 Model of the interaction between the SpoIVFB CBS domain and residues 96-99 of Pro-σ^K. The upper left panel shows the C chain of SpoIVFB and the Y chain of Pro-σ^K as in the upper right panel of Figure S7. Dashed lines indicate points of proximity (5-7 Å in each case) between the chains (distance between Cα atoms of indicated residues). The upper right panel shows a similar view rotated slightly, with residues 221-226 and 248 to the C-terminal end of SpoIVFB removed to better show the points of proximity. The lower right panel shows the same view with side chains added and space-filling atoms to illustrate packing. The lower left panel further illustrates packing.

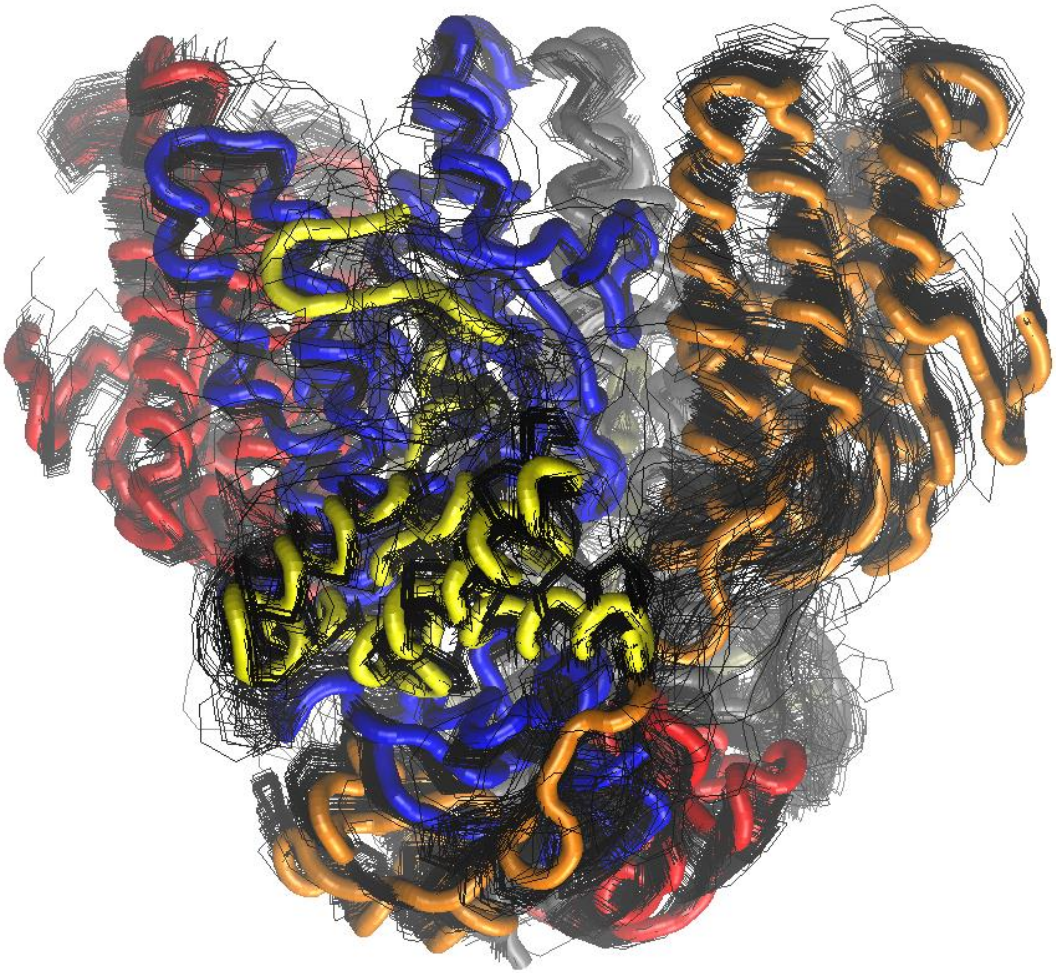

Figure S12 Variation of Cα-based models after restrained-based modeling (gray lines), and the model selected for further discussion (tubes colored by chains). In front is a chain of SpoIVFB (blue) interacting with a chain of Pro-σ^K (yellow).